High order multisymplectic Runge–Kutta methods

Robert I. McLachlan,[*] Brett N. Ryland,[†] and Yajuan Sun[‡]

Abstract

We study the spatial semidiscretizations obtained by applying Runge–Kutta (RK) and partitioned Runge–Kutta (PRK) methods to multisymplectic Hamiltonian partial differential equations. These methods can be regarded as multisymplectic hp-finite element methods for wave equations. All the methods we consider are multisymplectic; we determine their properties with regard to existence of solutions, dispersion, and order. The Lobatto IIIA–IIIB PRK method can lead to explicit ODEs and exhibits a surprisingly high order of 2 higher than the number of degrees of freedom per cell.

1 Introduction

Many conservative PDEs, such as nonlinear wave equations, have a multi-Hamiltonian formulation and an associated multisymplectic conservation law [5, 6]. As a generalization of symplectic integrators to PDEs, multisymplectic methods possess a discrete multisymplectic conservation law. They can be constructed by applying (possibly different) symplectic integrators in time and in space [15]. The (Preissman or Keller) box scheme, obtained by applying the implicit midpoint rule in space and time, is a simple and popular example. It has been shown that the box scheme has a remarkable ability to preserve the dispersion relation of any system of first order PDEs, up to a monotonic remapping of frequencies [4, 3, 2]. Amongst other things, this guarantees that it is free of (linear) parasitic waves and contributes to its robustness at comparably large space and time steps (see also [9]). This motivates our study of higher order methods with similarly good behaviour.

Although one of the guiding principles of multisymplectic geometry is that space and time are to be treated on an equal footing, in practice the boundary conditions break this symmetry. As symplectic time integration is relatively well-understood, we

concentrate here on symplectic space discretization; the same method can have very different properties when it is applied in space and in time.

A necessary condition for the stability of a Runge–Kutta spatial discretization is given in [14]. Not all methods that are stable for time integration, are stable for space discretization. Gauss–Legendre Runge–Kutta (GLRK) methods are unconditionally stable in both space and time, and we concentrate here on this family. (The box scheme is GLRK with one stage in space and one in time.) This class of multisymplectic integrators was introduced in [15] but its members with more than one stage have been little studied. The dispersion analysis of the box scheme was extended to GLRK by Frank, Moore, and Reich [8], who showed that a certain low-frequency portion of the dispersion relation is preserved up to a monotonic remapping of frequencies. Here, we study the dispersion relation further and find that GLRK smoothly captures the dispersion relation over the entire frequency range of the PDE, just like the box scheme.

Applying GLRK in space leads to linearly implicit ODEs for the dependent variables. This precludes the use of explicit time integrators. Further, we show that the mass matrix of these ODEs can be singular, depending on the method, the number of grid points, and the boundary conditions. An alternative for some PDEs which avoids this drawback is to discretize in space by a partitioned RK (PRK) method. For example, applying the simplest PRK method, leapfrog, to the wave equation $u_{tt} = u_{xx}$ [17] in space and time leads to the standard 5-point central difference discretization. For some PDEs it is possible to get explicit multisymplectic spatial discretizations of any order by PRK methods. Therefore, it is of interest to carry out the dispersion analysis for PRK discretizations as well. The methods of interest here are the Lobatto IIIA–IIIB methods. We show that the family of Lobatto IIIA–IIIB methods are stable and preserve a proper subset of the continuous frequency range. However, the mapping from continuous to discrete frequencies is not continuous, leading to a discrete dispersion relation with spurious jumps and critical points, and with a CFL-type stability restriction on explicit time integration.

The outline of the paper is as follows. In Section 2, we study the semidiscretization obtained by applying the RK method to multi-Hamiltonian PDEs in space. The semidiscretization leads to linearly implicit ODEs which may not be well defined (depending on the problem). Section 3 shows that the spatial discretization determined by applying the PRK method (Lobatto IIIA–IIIB) provides explicit ODEs for a certain class of multi-Hamiltonian PDEs. We study the numerical behavior of the semidiscretized system presented in Section 2 and 3 by dispersion analysis in Section 4. In Sections 5 and 6 we study the order behaviour of (P)RK semidiscretization. In particular, the Lobatto IIIA–IIIB method exhibits a surprisingly high order of 2 higher than the number of degrees of freedom per cell, a phenomenon we are able to prove only for a related method with specially chosen initial conditions.

2 Spatial discretization by Runge–Kutta methods

2.1 Discretization

We consider the multi-Hamiltonian PDE [15]

$$\mathsf{K}z_t + \mathsf{L}z_x = \nabla S(z), \quad z(x,t) \in \mathbb{R}^d, \tag{2.1}$$

in one space and one time dimension, where K and L are constant skew-symmetric matrices and $S(z)$ is a smooth function. This PDE has a multisymplectic conservation law

$$\omega_t + \kappa_x = 0, \quad \omega = \frac{1}{2}\mathsf{K}\mathrm{d}z \wedge \mathrm{d}z, \ \kappa = \frac{1}{2}\mathsf{L}\mathrm{d}z \wedge \mathrm{d}z. \tag{2.2}$$

The PDE and the conservation law are local; boundary conditions will be specified later where necessary. We concentrate here on the spatial semidiscretization. Consider an RK method with r stages and parameters a_{ij}, b_i, and c_i. Let Δx be the spatial mesh size (taken here to be constant, although this is not at all necessary). We introduce the nodal grid points x_i, spatial cells $[x_i, x_i + \Delta x]$, and stage grid points $x_i + c_j\Delta x$. The spatial cells are labelled by the discrete independent variable i; the dependent variable t remains continuous. The dependent variables associated with the spatial cell $[x_i, x_i + \Delta x]$ are the *node variables* $\bar{z} \in \mathbb{R}^d$ that approximate $z(x_i, t)$, stage variables $Z_j \in \mathbb{R}^d$, $j = 1, \ldots, r$ that approximate $z(x_i + c_j\Delta x, t)$, and *derivative variables* $X_j \in \mathbb{R}^d$, $j = 1, \ldots, r$, that approximate $z_x(x_i + c_j\Delta x, t)$. The independent variables i and t of $\bar{z}$, Z_j, and X_j are suppressed except where necessary. Thus there are $d(2r + 1)$ dependent variables per cell. The RK discretization applied to (2.1) in space is

$$Z_j = \bar{z}(i) + \Delta x \sum_{l=1}^{r} a_{jl}X_l, \quad j = 1, \ldots, r,$$

$$\bar{z}(i+1) = \bar{z}(i) + \Delta x \sum_{l=1}^{r} b_l X_l, \tag{2.3}$$

$$\mathsf{K}\partial_t Z_l + \mathsf{L}X_l = \nabla S(Z_l), \quad l = 1, \ldots, r.$$

Equations (2.3) form a set of implicit differential-algebraic equations which must be supplemented by appropriate initial and boundary conditions. Note that in contrast to time-discretization, where the stage values are determined by the RK method and a node value, in space discretization the stage values Z_j enter as dependent variables.

The node variables $\bar{z}$ and derivative variables X_j appear only linearly and algebraically, and can be eliminated as follows. First, apply the operator δ of forward difference across cells, $\delta\bar{z}_i := \bar{z}_{i+1} - \bar{z}_i$, to (2.3) and multiply by L to get

$$\delta\mathsf{L}Z_j = \delta\mathsf{L}\bar{z} + \Delta x \sum_{l=1}^{r} a_{jl}\delta\mathsf{L}X_l$$

$$= \Delta x \sum_{l=1}^{r} (b_l + a_{jl}\delta)\mathsf{L}X_l. \tag{2.4}$$

Second, eliminate the variables X_l from (2.4) using (2.3) to get

$$\delta \mathsf{L} Z_j = \Delta x \sum_{l=1}^{r} (b_l + a_{jl}\delta)(\nabla S(Z_l) - \mathsf{K}\partial_t Z_l)$$

or, in vector form,

$$\delta \mathsf{L} Z = \Delta x (\mathbf{1} b^\top + A\delta)(\nabla S(Z) - \mathsf{K}\partial_t Z), \qquad (2.5)$$

where $\mathbf{1}$ is a vector with all entries equal to 1. That is, any solutions of the DAE (2.3) imply that the linearly implicit ODE (2.5) holds for Z. If the operator $(\mathbf{1} b^\top + A\delta)$ is nonsingular then we formally invert it to write

$$\mathsf{K}\partial_t Z + (\Delta x)^{-1}(\mathbf{1} b^\top + A\delta)^{-1}\delta \mathsf{L} Z = \nabla S(Z). \qquad (2.6)$$

The effect of the RK spatial discretization is to approximate the operator $\frac{\partial}{\partial x}$ by the (in general, implicit) finite difference operator $(\Delta x)^{-1}(\mathbf{1} b^\top + A\delta)^{-1}\delta$ that does not depend on the PDE in question. It only sees the RK coefficients and the boundary conditions. Because the approximation is linear, we can understand most of its properties from the behaviour of the RK method applied to linear differential equations, an extremely well-understood subject. If L is singular, then (assuming for convenience that L is in Darboux form) some of the components of the PDE (2.1) contain no x-derivatives and there is no reason to discretize this in x. However, we see from the above form of the semidiscretization that the terms vanishing in the PDE also vanish in the semidiscretization. Similarly, if K is singular, then some of the components of the PDE correspond to constraints. In (2.6), the same components of the PDE correspond to constraints on Z. In some applications, these constraints will be eliminated both in the PDE and in the semidiscretization, leading to $r \times \mathrm{rank}(\mathsf{K})$ ODEs per cell. In other words, the RK spatial discretization does not affect the (K, L) geometry of the multi-Hamiltonian PDE.

Note that the formulation (2.6) differs in the case $r = 1$ from the standard presentation of the box method. In the box method, we take the implicit midpoint rule together with Eq. (2.3), but eliminate X_1 and Z_1 by using $Z_1(i) = M\bar{z}(i) := (\bar{z}(i) + \bar{z}(i+1))/2$, to get

$$\mathsf{K}M\partial_t\bar{z} + \delta \mathsf{L}\bar{z} = \nabla S(M\bar{z}). \qquad (2.7)$$

This elimination of the stage variables is only possible when $r = 1$. The box method and the RK method ($r = 1$) which obey identical equations on each cell, but, in different implementations, may differ depending on how the boundary and initial conditions are imposed.

2.2 The mass matrix of the RK discretization

After imposing some (linear) boundary conditions, we have seen in Eq. (2.6) that the RK spatial discretization leads to a linearly implicit ODE of the form $M\partial_t Z = f(Z)$, where M is a mass matrix. If M is nonsingular, then this is always equivalent to an ODE; if M is singular, it is a differential–algebraic equation whose well-posedness requires extensive further analysis and which depends on f. Although we have not found this

point addressed anywhere in the literature, it seems to have been implicitly assumed that GLRK spatial discretization always yields a nonsingular M and hence that the method is well-posed in the simplest sense. We now show that this is not the case; even for periodic boundary conditions, in some sense the simplest case, M is often singular.

Starting from Eq. (2.3), imposing periodic boundary conditions with N spatial cells numbered from 1 to N and eliminating X_l (but not $\bar{z}(i)$) gives, with $Z(i) = (Z_1(i), \ldots, Z_r(i))^\top \in \mathbb{R}^{r \times d}$, the linearly implicit ODE

$$
\begin{bmatrix}
\Delta x A \otimes I_d & & & \mathbf{1}_r \otimes I_d & & \\
& \ddots & & & \ddots & \\
& & \Delta x A \otimes I_d & & & \mathbf{1}_r \otimes I_d \\
\hline
\Delta x b^\top \otimes I_d & & & I_d & & -I_d \\
& \ddots & & & \ddots & -I_d \\
& & \Delta x b^\top \otimes I_d & -I_d & & I_d
\end{bmatrix}
\begin{bmatrix}
\nabla S(Z(1)) - \mathsf{K}\partial_t Z(1) \\
\vdots \\
\nabla S(Z(N)) - \mathsf{K}\partial_t Z(N) \\
\hline
\mathsf{L}\bar{z}(1) \\
\vdots \\
\mathsf{L}\bar{z}(N)
\end{bmatrix}
=
\begin{bmatrix}
\mathsf{L}Z(1) \\
\vdots \\
\mathsf{L}Z(N) \\
\hline
0 \\
\vdots \\
0
\end{bmatrix}.
$$
(2.8)

Theorem 2.1. *For a GLRK spatial discretization applied to the multi-Hamiltonian PDE (2.1) with periodic boundary conditions, the matrix on the left-hand side of (2.8) is nonsingular iff the number of stages r, and the number of grid points, N, are both odd.*

Proof. The determinant of a block matrix in which at least one block, say A, is nonsingular, can be calculated by

$$
\det \begin{bmatrix} A & B \\ C & D \end{bmatrix} = \det(A)\det(D - CA^{-1}B).
$$
(2.9)

Since (2.1) is discretized by a GLRK method, the matrix A in (2.8) is of full rank, therefore the upper left block of the matrix in (2.8) is nonsingular and has the determinant $(\Delta x)^{rNd}\det(A)^{Nd}$. Also, the block matrix product $CA^{-1}B$, where A, B and C are the blocks in (2.9) matching those of (2.8), is I_{Nd} times the scalar $b^\top A^{-1}\mathbf{1}$.

Now, the stability function for a RK method is given by [12]

$$
R(w) = 1 + wb^\top (I - wA)^{-1}\mathbf{1},
$$
(2.10)

so that

$$
\lim_{w \to \infty} R(w) = 1 - b^\top A^{-1}\mathbf{1}.
$$
(2.11)

On the other hand, for the r-stage GLRK method, the stability function is the diagonal Padé approximation

$$
R(w) = P_{rr}(w) = \frac{N_{rr}(w)}{N_{rr}(-w)},
$$

so that

$$
\lim_{w \to \infty} R(w) = (-1)^r.
$$
(2.12)

5

Comparing these two limits gives $1 - b^\top A^{-1}\mathbf{1} = (-1)^r$, and thus we obtain

$$b^\top A^{-1}\mathbf{1} = \begin{cases} 0, & \text{if } r \text{ is even;} \\ 2, & \text{if } r \text{ is odd.} \end{cases} \tag{2.13}$$

Hence, if r is even, the block matrix product $D - CA^{-1}B$ is the $Nd \times Nd$ matrix

$$\begin{bmatrix} I_d & -I_d & \\ & \ddots & -I_d \\ -I_d & & I_d \end{bmatrix}$$

which is always singular. But when r is odd, this block matrix product is the $Nd \times Nd$ matrix

$$\begin{bmatrix} -I_d & -I_d & \\ & \ddots & -I_d \\ -I_d & & -I_d \end{bmatrix}$$

which is singular when N is even and nonsingular (with determinant is $(-2)^d$) when N is odd.

Therefore, the matrix on the left-hand side of (2.8) is nonsingular (with determinant $(-2)^d(\Delta x)^{rNd}\det(A)^{Nd}$) iff both r and N are odd. $\qquad\square$

When $r = 1$ and N is even, the singular mode is the familiar sawtooth $Z(j) = (-1)^j$. When $r > 1$, the nullspace is higher dimensional. It is still possible that the DAE (2.3) could have a solution in some cases when N or r is even. The singular modes are high frequency (like the sawtooth) and are typically small and one could consider projecting them out. However, their presence is certainly an obstacle to the more widespread use of GLRK in space. Indeed, most published numerical results use $r = 1$ and N odd.

One can consider studying the structure of the system (2.3) with, e.g., Dirichlet or Neumann boundary conditions. However, now the structure depends on all the data of the PDE $(\mathsf{K}, \mathsf{L}, S)$. Even for restricted problem classes like the nonlinear wave equation, we have not been able to find a systematic formulation which leads to a nonsingular linearly implicit ODE.

2.3 Dispersion analysis

The linear multi-Hamiltonian PDE

$$\mathsf{K}z_t + \mathsf{L}z_x = \mathsf{S}z \tag{2.14}$$

has periodic solutions of the form

$$z(x,t) = \exp(\mathrm{i}(kx + \omega t))y \tag{2.15}$$

iff

$$\mathcal{D}(\omega, k) := \det(\mathrm{i}\omega\mathsf{K} + \mathrm{i}k\mathsf{L} - \mathsf{S}) = 0. \tag{2.16}$$

This establishes the dispersion relation between the frequency ω and the wave number k.

Theorem 2.2. *[8] Let $\mathcal{D}(\omega, k) = 0$ for the PDE (2.14). Then the semidiscretization of (2.14) by a Runge–Kutta method in space with stability function $R(w)$ has solutions of the form*

$$\bar{z}(i) = \exp(\mathrm{i}\omega t) \exp(\mathrm{i}Ki\Delta x)y, \, Z_j(i) = \exp(\mathrm{i}\omega t) \exp(\mathrm{i}Ki\Delta x)Y_j, \quad j = 1, \ldots, r, \quad (2.17)$$

where

$$Y_j = \left((I - \mathrm{i}k\Delta x A)^{-1}\mathbf{1}\right)_j y. \tag{2.18}$$

and

$$\exp(\mathrm{i}K\Delta x) = R(\mathrm{i}k\Delta x). \tag{2.19}$$

From (2.19), we have the following corollary for the semidiscretized ODEs (2.6).

Corollary 2.1. *The error of the discrete dispersion relation is*

$$k\Delta x - K\Delta x = \mathcal{O}((k\Delta x)^{2r+1}) \tag{2.20}$$

as $k\Delta x \to 0$. That is, the dispersion order of r-stage GLRK in space is $2r$.

Proof. For fixed r, when $k\Delta x \to 0$ we know from [12] that

$$R(\mathrm{i}k\Delta x) = \exp(\mathrm{i}k\Delta x) - \mathrm{i}e_r(k\Delta x)^{2r+1} + \mathcal{O}((k\Delta x)^{2r+2}),$$

where $e_r = \frac{r!^2}{2r!(2r+1)!}$. $\qquad\qquad\square$

That is, the dispersion order of any RK method in space is equal to its classical order.

It is known that $|R(\mathrm{i}k\Delta x)| = 1$ for all k and that the phase $\phi(\mathrm{i}k\Delta x)$ can be chosen so that

$$R(\mathrm{i}k\Delta x) = \mathrm{e}^{i\phi(k\Delta x)}$$

where the phase

$$\phi\colon (-\infty, \infty) \to (-r\pi, r\pi)$$

is a monotonically increasing diffeomorphism [10]. The asymptotic behaviour of $R(w)$ and $R(rw)$ as $r \to \infty$ is developed in [14]. Thus, to each fundamental discrete frequency $K\Delta x \in (-\pi, \pi)$ there correspond exactly r values of the continuous frequency $k\Delta x$. These are the r modes supported on each cell, corresponding to the r dependent variables $Z_1, \ldots, Z_r$. The traditional viewpoint is that the smallest value of $k\Delta x$ is the wave that the discretization approximates and that the other $r - 1$ values of $k\Delta x$ correspond to spurious waves (see, e.g., [7]). This is not correct. Another description is given in [8], where it is argued on pp. 270–271 that the value of $k\Delta x$ should be limited to give a unique $K\Delta x \in (-\pi, \pi)$, resulting in just one numerical mode per cell. This is not correct. Not only must there be r modes supported on each cell, for stability reasons, the $r - 1$ higher-frequency modes smoothly approximate the entire spectrum of the PDE. Our interpretation of Theorem 2.2, together with the known properties of $R(w)$ for GLRK, is the following.
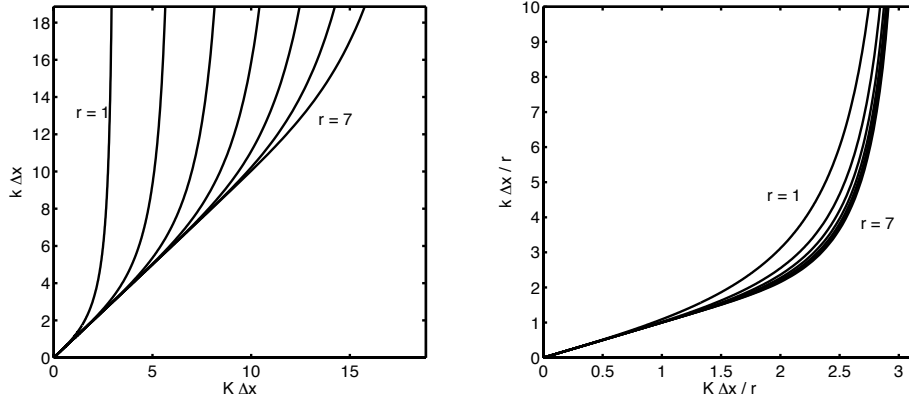
Figure 2.1: Left: Mapping between continuous ($k\Delta x$) and discrete ($K\Delta x$) frequencies for GLRK methods with $r = 1, 2, \ldots, 7$ stages. Right: Both frequencies scaled by r to show the rapid convergence as $r \to \infty$ and the uniform convergence of $k\Delta x/r$ to $K\Delta x/r$ for arguments less than 2, that is, discrete frequencies up to $2r/\Delta x$ are asymptotically exact.

Corollary 2.2. *To each $k \in (-\infty, \infty)$ there is a unique $K\Delta x = \phi(k\Delta x) \in (-r\pi, r\pi)$ such that for each ω satisfying the continuous dispersion relation $\mathcal{D}(\omega, k) = 0$, the GLRK semidiscretization has a discrete periodic solution given by (2.17), (2.18). Conversely, for each $K\Delta x \in (-\pi, \pi)$, to each of the r solutions $(K\Delta x, k\Delta x)$ to (2.19) an integer multiple of 2π can be added to $K\Delta x$ so that the solution takes the form $K\Delta x = \phi(k\Delta x)$. The GLRK semidiscretization preserves the entire dispersion relation of any multi-Hamiltonian PDE, up to a diffeomorphic remapping of frequencies, for all Δx, with no spurious or parasitic waves. The sign of the phase and group velocities are preserved for all frequencies and for all Δx.*

From now on we will use the choice of phase given by $K\Delta x = \phi(k\Delta x)$. The mapping between continuous and discrete frequencies for GLRK methods applied to the linear wave equation is shown in Fig. 2.1. It is shown in [14] that $K\Delta x/r \to k\Delta x/r$ as $r \to \infty$ for $K\Delta x/r < 2$. This is the highest possible frequency that can be represented on the grid based on the Nyquist sampling theorem and the maximum grid spacing $c_{j+1} - c_j$, which tends to $\pi/(2r)$ as $r \to \infty$. Although Corollary 2.2 determines the semidiscrete dispersion relation for any multi-Hamiltonian PDE, Fig. 2.1 also displays the semidiscrete dispersion relation for the linear wave equation directly (in that case $\omega = \pm k$).

Note that the higher-frequency solutions with $K\Delta x \notin (-\pi, \pi)$ all map onto the same function on the nodal grid points, namely $\bar{z}(i)$ in (2.17). However, they do not all map onto the same function on the stage grid points, and it is these that are the active dependent variables.

These modes are described by Y_j introduced in (2.18). From the point of view of dispersion analysis, these are irrelevant; all that matters is the spectrum of the linear

8

ODEs. However, to compare the computational modes to the analytic modes, or to compare the numerical solution to the exact solution, we do need the Y_j. For the box scheme, the grid is uniform, and the computational modes $\exp(iKm\Delta x)y$ coincide with the analytic modes $\exp(iKx)$ evaluated at the grid points $x = x_m$. In this case the dispersion relation carries all the information about the discretization. For nonuniform grids, the computational modes do not coincide with the analytic modes evaluated on the grid, so we also need to study the spatial structure of the computational modes. In the following example we study these for the 2-stage GLRK method.

Example 2.1. *For the 2-stage GLRK method, the stability function is $R(w) = \frac{12+6w+w^2}{12-6w+w^2}$, so $\exp(iK\Delta x) = R(ik\Delta x)$ leads to*

$$\tan \frac{K\Delta x}{2} = \frac{k\Delta x}{2 - \frac{1}{6}(k\Delta x)^2}. \tag{2.21}$$

It is known from (2.18) that the numerical mode Y_j can be calculated by

$$Y = (I - ik\Delta x A)^{-1}\mathbf{1}y$$
$$= \frac{1}{12 - 6(ik\Delta x) + (ik\Delta x)^2}\begin{pmatrix} 12 - 2\sqrt{3}ik\Delta x \\ 12 + 2\sqrt{3}ik\Delta x \end{pmatrix}y. \tag{2.22}$$

The numerical modes are defined up to an overall constant. We can scale the amplitudes to achieve $|Y_1| = 1$ and scale the phases so that $\arg Y_1 + \arg Y_2 = 0$. From (2.22), we know $|Y_1| = |Y_2|$. Therefore, we only need to keep track of the relative phases of $Y_{1,2}$. It follows from (2.22) that

$$\frac{Y_2}{Y_1} = \frac{12 + 2\sqrt{3}ik\Delta x}{12 - 2\sqrt{3}ik\Delta x},$$

so

$$\tan \phi = \frac{\sqrt{3}}{6}k\Delta x,$$

where $2\phi = \arg(Y_2/Y_1)$. This is most conveniently written in terms of K using the double angle formula

$$\tan 2\phi = \frac{2\tan\phi}{1 - \tan^2\phi} = \frac{2\sqrt{3}}{3}\frac{k\Delta x}{2 - \frac{1}{6}(k\Delta x)^2} = \frac{2\sqrt{3}}{3}\tan\frac{K\Delta x}{2}.$$

This can be compared to the values of the eigenfunctions of the continuous problem evaluated at the stage grid points, normalized by their value at the cell midpoints, namely $e^{(i(c_j - \frac{1}{2})K\Delta x)}$. With $c_2 - \frac{1}{2} = \frac{\sqrt{3}}{6}$, this gives the phase for the continuous problem as $\frac{\sqrt{3}}{6}K\Delta x$, whereas the phase for the RK discretization is

$$\phi = \frac{\sqrt{3}}{6}K\Delta x - \frac{\sqrt{3}}{216}(K\Delta x)^3 + \mathcal{O}(K\Delta x)^5,$$

so the continuous and discrete phases of the eigenfunctions agree in the limit $K\Delta x \to 0$ (as was to be expected), but are not identical. However, note that the discrete phase is
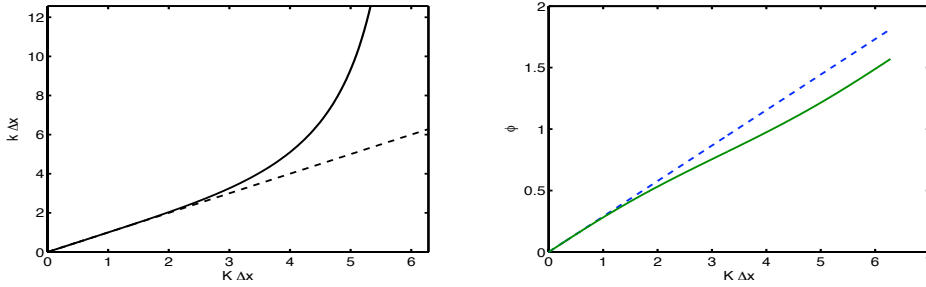
9

Figure 2.2: Left: Dispersion relation for the 2-stage GLRK method. The dashed line is $k = K$. Each cell of width Δx contains two dependent variables, Z_1 and Z_2, and supports two modes: one is a low-frequency mode in $[0, \pi)$ and one is a high-frequency mode in $[\pi, 2\pi)$. Right: The discrete phase $\phi = \arg(Z_2/Z_1)/2$. The dashed line is the value for the 'exact' Fourier mode, $\phi = \frac{\sqrt{3}}{6} K \Delta x$.

a good approximation to the continuous phase over the whole frequency range $K\Delta x \in (-2\pi, 2\pi)$ (equivalently, $k \in (-\infty, \infty)$). The phase error reaches a maximum at the very highest frequencies $K\Delta x \to 2\pi$, where $\phi = \pi/2 \approx 1.57$ compared to the continuous phase $\pi/\sqrt{3} \approx 1.81$. Fig. 2.2 shows the dispersion relation and the relative discrete phase in correspondence with the continuous ones.

Another way of looking at the high frequency behaviour is to let $k \to \infty$ in (2.22), which gives (with a different normalization)

$$Y \to A^{-1}\mathbf{1} \propto \begin{pmatrix} -1 \\ 1 \end{pmatrix}.$$

In other words, these highest-frequency modes look very much like a sawtooth wave, just as they do when $k \to \infty$ for the midpoint rule.

We now repeat the calculation of Example 2.1 for $r = 3, \ldots, 7$, numerically rather than analytically. For a given r, let $U_i = Y_i/Y_1$. Fig. 2.3 shows the dependence of $\arg(U_i)$ on $K\Delta x/r$, and Fig. 2.4 shows the dependence of $|U_i|$ on $K\Delta x/r$ for the r modes $i = 1, \ldots, r$. By symmetry, some of the modes coincide. Two immediate observations are that (i) the arguments appear to be much more accurate over the whole frequency range than the moduli, which become much less than 1 (the 'exact' value) in the high frequency range; and (ii) U_i appears to converge uniformly to the continuous value only in the frequency range $K\Delta x/r < \pi/2$, in contrast to the dispersion relation which has been proved to converge uniformly in $K\Delta x/r < 2$.

From (2.18), the high-frequency limit is $\lim_{k\Delta x \to \infty} Y_j \propto A^{-1}\mathbf{1}$. This quantity is determined in the following proposition.
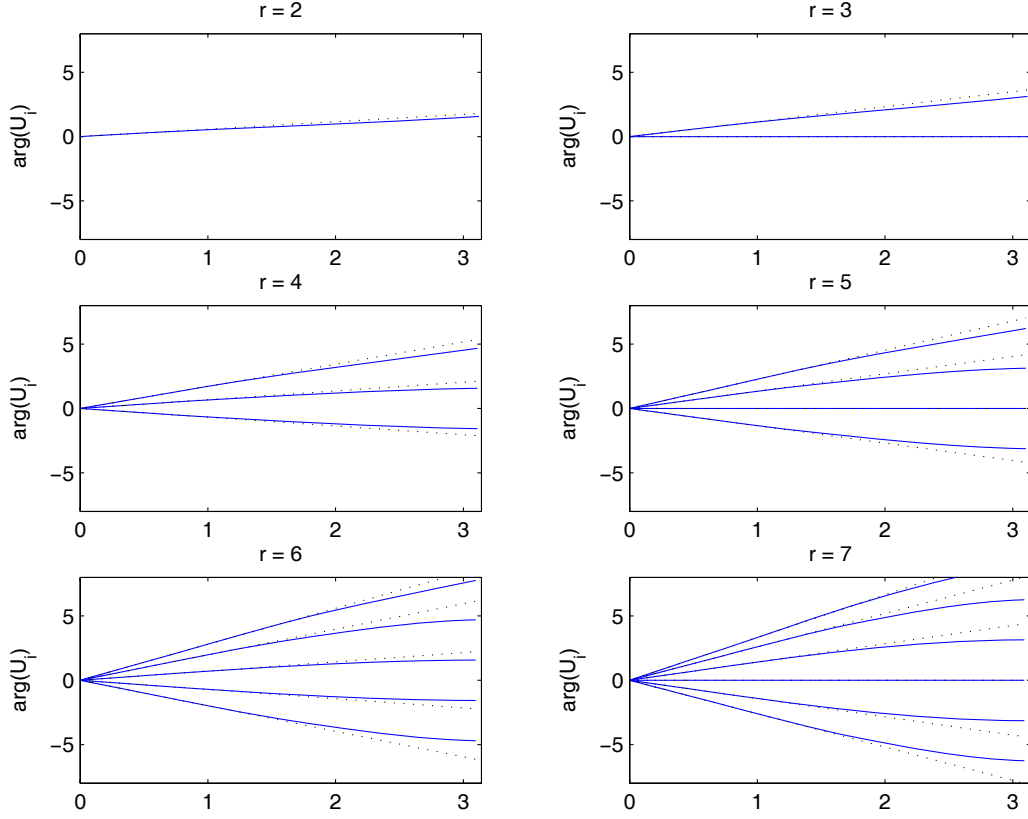
Figure 2.3: Discrete phase $\{\arg(U_i)\}_{i=2}^r$ for the low-frequency mode in $[0, \pi)$ with respect to $K\Delta x/r$ for GLRK of $r = 2, \ldots, 7$ stages. The dashed lines are $\arg(U_i) = (c_i - 1/2)K\Delta x$ corresponding to the 'exact' phases.

Proposition 2.1. *For the r-stage GLRK method (A, b, c), we have*

$$(A^{-1}\mathbf{1})_i = (-1)^{r-1}\left(\prod_{j=1}^r c_j\right)^{-1}\prod_{l \neq i}(c_i - c_l), \quad i = 1, \ldots, r. \tag{2.23}$$

Proof. For the r-stage GLRK method (A, b, c), the simplifying assumption $B(2r)$ is satisfied. That is,

$$\sum_{j=1}^r a_{ij}c_j^{k-1} = \frac{1}{k}c_i^k = \int_0^{c_i} x^{k-1}dx, \quad 1 \leq i, k \leq r. \tag{2.24}$$

Denote $P(x) = \prod_{j=1}^r (x - c_j)$. It is known that $P(c_i) = 0$, $i = 1, \ldots, r$, and $P'(x) =$
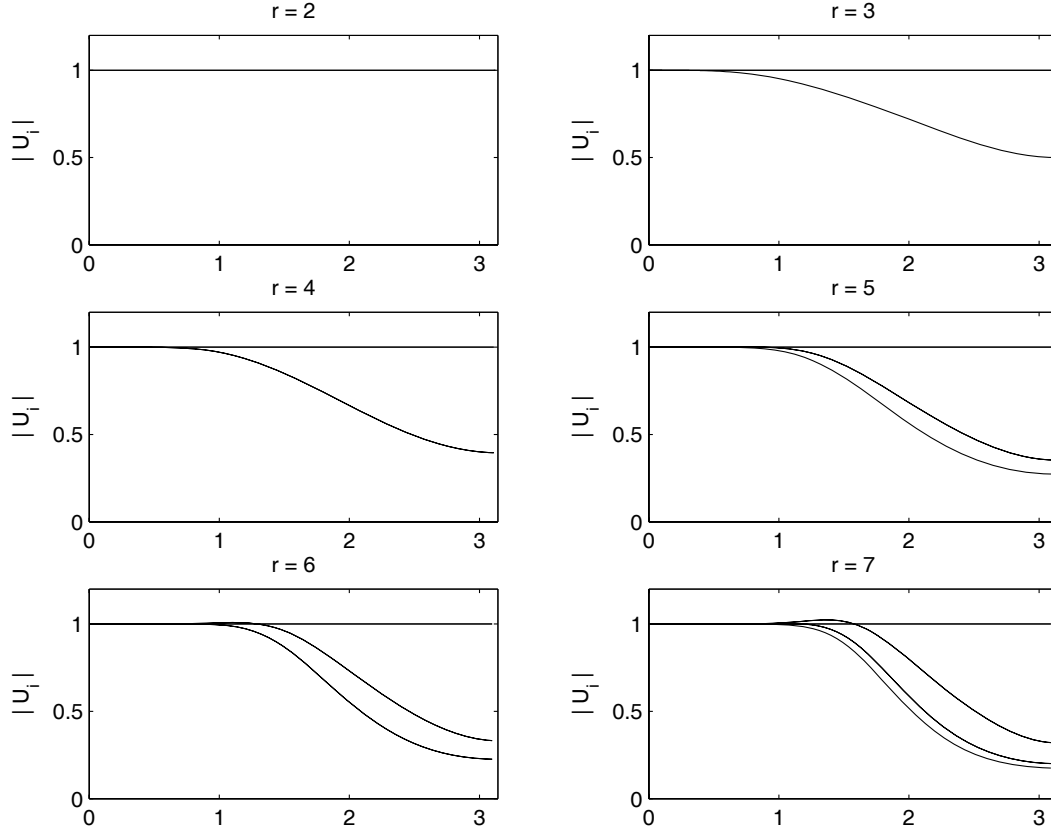
11

Figure 2.4: Norms of U_i, $\{|U_i|\}_{i=2}^r$ for the low-frequency mode in $[0, \pi)$ with respect to $K\Delta x/r$ for GLRK of $r = 2, \ldots, 7$ stages.

$\sum_{i=1}^{r} \prod_{j \neq i} (x - c_j)$. It follows from (2.24) that

$$
\begin{aligned}
\sum_{k=1}^{r} a_{ik} \prod_{j \neq k} (c_k - c_j) &= \sum_{k=1}^{r} a_{ik} P'(c_k) \\
&= \int_0^{c_i} P'(x) dx \\
&= (-1)^{r-1} \prod_{j=1}^{r} c_j, \text{ for } i = 1, \ldots, r.
\end{aligned}
$$

Taking the inverse of A gives Eq. (2.23). $\qquad\qquad\qquad\qquad\qquad\qquad\square$

From the proposition, we see that the components of $A^{-1}\mathbf{1}$ oscillate in sign like a sawtooth wave.

2.4   Global error

The dispersion analysis in the previous section did not require any connection between the stage values $Z_j(i)$ and the continuous solution $z(x)$, although we used $Z_j(i) \approx z(x_i + c_j \Delta x)$ as an aid to visualizing the discrete modes. Note that the stage order of GLRK method, which is the order of Z_j as an approximation of $z(t_i + c_j \Delta t)$ when used as a time integrator, is $r+1$ [11]. Since Z_j are the dependent variables, we cannot attain more than this order. In the following theorem we establish that the global order is at least r for a very large family of hyperbolic PDEs.

Theorem 2.3. *Assume that the multi-Hamiltonian system of PDEs (2.1) is hyperbolic with K non-degenerate and that the nonlinear term $\nabla S(z)$ satisfies a Lipschitz condition. Apply the r-stage symplectic GLRK method to the multi-Hamiltonian system in space, with periodic boundary condition, then for all $T > 0$ there exists a constant C such that*

(i) when $r = 1$, the global error at the stage values is

$$\left(\sum_{i=1}^{N} \Delta x |z(x_i + \frac{1}{2}\Delta x, t) - Z_1(i,t)|^2 \right)^{1/2} \leq C(\Delta x)^2, \quad t \in [0, T];$$

(ii) when $r > 1$, the global error at the stage values is

$$E := \left(\sum_{i=1}^{N} \sum_{j=1}^{r} \Delta x b_j |z(x_i + c_j \Delta x, t) - Z_j(i,t)|^2 \right)^{1/2} \leq C(\Delta x)^r, \quad t \in [0, T], \tag{2.25}$$

where $Z_j(i,t)$ is the numerical solution and $z(x_i + c_j \Delta x, t)$ is the exact solution at the stage grid points $x_i + c_j \Delta x$.

Proof. (i) When $r = 1$, (2.3) is the semi-discretized box scheme which is written as

$$\mathsf{K} \partial_t Z_1(i,t) + \mathsf{L} X_1(i,t) = \nabla S(Z_1) \tag{2.26}$$

with $Z_1(i,t) = (\bar{z}(i+1,t) + \bar{z}(i,t))/2$ and $X_1(i,t) = (\bar{z}(i+1,t) - \bar{z}(i,t))/\Delta x$. Let $e(i,t) = \bar{z}(i,t) - z(x_i,t)$. It is clear that

$$\begin{aligned}
\mathsf{P} \partial_t \frac{e(i+1,t) + e(i,t)}{2} &+ \mathsf{P}\mathsf{K}^{-1}\mathsf{L} \frac{e(i+1,t) - e(i,t)}{\Delta x} \\
&= \mathsf{P}\mathsf{K}^{-1} \left(\nabla S(Z_1) - \nabla S \left(\frac{z(x_i + \Delta x, t) + z(x_i, t)}{2} \right) \right) + \mathcal{O}(\Delta x^2).
\end{aligned} \tag{2.27}$$

As the multi-Hamiltonian system (2.1) is hyperbolic, there exists P such that $\mathsf{K}^{-1}\mathsf{L} = \mathsf{P}^{-1}\mathsf{D}\mathsf{P}$ with D the diagonal matrix.

13

Left-multiplying $(\mathsf{P}\mathcal{E})^\top \triangleq (\mathsf{P}(e(i+1,t)+e(i,t))/2)^\top$ on both sides of (2.27), we gain that

$$\frac{1}{2}\partial_t\left((\mathsf{P}\mathcal{E})^\top\mathsf{P}\mathcal{E}\right) + \frac{e(i+1,t)^\top\mathsf{P}^\top\mathsf{D}\mathsf{P}e(i+1,t) - e(i,t)^\top\mathsf{P}^\top\mathsf{D}\mathsf{P}e(i,t)}{2\Delta x}$$
$$= (\mathsf{P}\mathcal{E})^\top\mathcal{O}(\Delta x^2) + (\mathsf{P}\mathcal{E})^\top\mathsf{P}\mathsf{K}^{-1}\mathsf{P}^\top\nabla(\bar{S}(\mathsf{P}Z_1) - \bar{S}(\mathsf{P}z_c)), \tag{2.28}$$

where $z_c = (z(x_i+\Delta x,t)+z(x_i,t))/2$, $\bar{S}(\mathsf{P}Z) = S(Z)$. By applying the Cauchy–Schwarz inequality and Young's inequality to the first term, and the mean value theorem to the last term on right side of the above equality, it thus follows that

$$\frac{1}{2}\partial_t\left((\mathsf{P}\mathcal{E})^\top\mathsf{P}\mathcal{E}\right) + \frac{e(i+1,t)^\top\mathsf{P}^\top\mathsf{D}\mathsf{P}e(i+1,t) - e(i,t)^\top\mathsf{P}^\top\mathsf{D}\mathsf{P}e(i,t)}{2\Delta x}$$
$$\leq \frac{1}{2}(\mathsf{P}\mathcal{E})^\top\mathsf{P}\mathcal{E} + \mathcal{O}(\Delta x^4) + (\mathsf{P}\mathcal{E})^\top\mathsf{P}\mathsf{K}^{-1}\mathsf{P}^\top\bar{S}''(\xi)\mathsf{P}\mathcal{E}. \tag{2.29}$$

Summing (2.29) over i from 1 to N and applying the periodic boundary condition, the second term on left side of (2.29) disappears, leading to

$$\frac{1}{2}\frac{d}{dt}\sum_{i=1}^{N}(\mathsf{P}\mathcal{E})^\top\mathsf{P}\mathcal{E} \leq \lambda_{\max}\sum_{i=1}^{N}(\mathsf{P}\mathcal{E})^\top\mathsf{P}\mathcal{E} + \sum_{i=1}^{N}\frac{1}{2}(\mathsf{P}\mathcal{E})^\top\mathsf{P}\mathcal{E} + \mathcal{O}(\Delta x^3), \tag{2.30}$$

where $\lambda_{\max}$ is the upper bound of the maximum eigenvalues of symmetric matrix $1/2(\mathsf{A}+\mathsf{A}^\top)$ with $\mathsf{A} \triangleq \mathsf{P}\mathsf{K}^{-1}\mathsf{P}^\top\bar{S}''(\xi)$. By Gronwall's inequality, it follows from (2.30) that

$$\sum_{i=1}^{N}\Delta x(\mathsf{P}\mathcal{E})^\top\mathsf{P}\mathcal{E} \leq C(\Delta x^4).$$

This proves part (i).

(ii) When $r > 1$, it is known that the coefficients (a_{ij}, b_i, c_i) of the r-stage GLRK method satisfy the simplifying conditions $B(2r)$ and $C(r)$. The condition $B(2r)$ leads to

$$z(x_i+\Delta x,t) = z(x_i,t) + \Delta x\int_0^1 z_x(x_i+\xi\Delta x,t)d\xi$$
$$= z(x_i,t) + \Delta x\sum_{k=1}^{r}b_k z_x(x_i+c_k\Delta x,t) + \mathcal{O}(\Delta x^{2r+1}). \tag{2.31}$$

Similarly, the condition $C(r)$ leads to

$$z(x_i+c_j\Delta x,t) = z(x_i,t) + \Delta x\int_0^{c_j} z_x(x_i+\xi\Delta x,t)d\xi$$
$$= z(x_i,t) + \Delta x\sum_{k=1}^{r}a_{jk} z_x(x_i+c_k\Delta x,t) + \mathcal{O}(\Delta x^{r+1}). \tag{2.32}$$

14

Define $E_j(i,t) = Z_j(i,t) - z(x_i + c_j\Delta x, t)$, $e(i,t) = \bar{z}(i,t) - z(x_i, t)$, and $\partial_x E_j(i,t) = X_j(i,t) - z_x(x_i + c_j\Delta x, t)$. Subtracting (2.3) from (2.31) and (2.32), we get that

$$E_j(i,t) = e(i,t) + \Delta x \sum_{l=1}^{r} a_{jl}\partial_x E_l(i,t) + \mathcal{O}(\Delta x^{r+1}), \quad j = 1,\ldots,r,$$

$$e(i+1,t) = e(i,t) + \Delta x \sum_{l=1}^{r} b_l\partial_x E_l(i,t) + \mathcal{O}(\Delta x^{2r+1}),$$

(2.33)

and

$$\mathsf{P}\partial_t E_l(i,t) + \mathsf{P}\mathsf{K}^{-1}\mathsf{L}\partial_x E_l(i,t) = \mathsf{P}\mathsf{K}^{-1}(\nabla S(Z_l) - \nabla S(z)), \quad l = 1,\ldots,r. \quad (2.34)$$

From the second equality of (2.33) we obtain

$$e(i+1,t)^{\top}\mathsf{P}^{\top}\mathsf{DP}e(i+1,t) = \left(e(i,t) + \Delta x \sum_{l=1}^{r} b_l\partial_x E_l\right)^{\top}\mathsf{P}^{\top}\mathsf{DP}\left(e(i,t) + \Delta x \sum_{l=1}^{r} b_l\partial_x E_l\right)$$

$$+ \mathcal{O}(\Delta x^{2r+1})$$

$$= e(i,t)^{\top}\mathsf{P}^{\top}\mathsf{DP}e(i,t) + \Delta x^2 \sum_{l,m=1}^{r} b_l b_m \partial_x E_l^{\top}\mathsf{P}^{\top}\mathsf{DP}\partial_x E_m$$

$$+ 2\Delta x \sum_{l=1}^{r} b_l\partial_x E_l^{\top}\mathsf{P}^{\top}\mathsf{DP}e(i,t) + \mathcal{O}(\Delta x^{2r+1}).$$

(2.35)

From the first equality of (2.33),

$$e(i,t) = E_j(i,t) - \Delta x \sum_{l=1}^{r} a_{jl}\partial_x E_l(i,t) + \mathcal{O}(\Delta x^{r+1}). \quad (2.36)$$

Substituting this into the third term of (2.35) leads to

$$e(i+1,t)^{\top}\mathsf{P}^{\top}\mathsf{DP}e(i+1,t) = e(i,t)^{\top}\mathsf{P}^{\top}\mathsf{DP}e(i,t) + 2\Delta x \sum_{l=1}^{r} b_l\partial_x E_l^{\top}\mathsf{P}^{\top}\mathsf{DP}E_l$$

$$+ \Delta x^2 \sum_{l,m=1}^{r} (b_l b_m - b_l a_{lm} - b_m a_{ml})\partial_x E_l^{\top}\mathsf{P}^{\top}\mathsf{DP}\partial_x E_m$$

$$+ 2\sum_{l=1}^{r} b_l\partial_x E_l^{\top}\mathbf{1}\mathcal{O}(\Delta x^{r+2}) + \mathcal{O}(\Delta x^{2r+1}).$$

(2.37)

Applying the periodic boundary condition, the second equality of (2.33) gives

$$\sum_{i=1}^{N}\sum_{l=1}^{r} b_l\partial_x E_l = \mathcal{O}(\Delta x^{2r-1}).$$

15

Substituting this into (2.37) leads to

$$\sum_{i=1}^{N}\sum_{l=1}^{r} b_l \partial_x E_l^\top \mathsf{P}^\top \mathsf{DP} E_l = \mathcal{O}(\Delta x^{2r-1}). \tag{2.38}$$

As $\mathsf{K}^{-1}\mathsf{L} = \mathsf{P}^{-1}\mathsf{DP}$, multiplying $E_l(i,t)^\top$ from left on both sides of (2.34), it reads that

$$\frac{1}{2}\frac{d}{dt}\sum_{l=1}^{r} b_l(\mathsf{P}E_l)^\top \mathsf{P}E_l + \sum_{l=1}^{r} b_l(\mathsf{P}E_l)^\top \mathsf{DP}\partial_x E_l = \sum_{l=1}^{r} b_l(\mathsf{P}E_l)^\top \mathsf{P}\mathsf{K}^{-1}\mathsf{P}^\top(\nabla\bar{S}(\mathsf{P}Z_l) - \nabla\bar{S}(\mathsf{P}z)). \tag{2.39}$$

Taking the sum of above equality w.r.t i from 1 to N, together with (2.38), we conclude that

$$\frac{1}{2}\frac{d}{dt}\sum_{i=1}^{N}\sum_{l=1}^{r} b_l(\mathsf{P}E_l)^\top \mathsf{P}E_l = \sum_{i=1}^{N}\sum_{l=1}^{r} b_l(\mathsf{P}E_l)^\top \mathsf{P}\mathsf{K}^{-1}P^\top \nabla^2\bar{S}(\xi)\mathsf{P}E_l + \mathcal{O}(\Delta x^{2r-1})$$

$$\leq \lambda_{\max}\sum_{i=1}^{N}\sum_{l=1}^{r} b_l(\mathsf{P}E_l)^\top \mathsf{P}E_l + \mathcal{O}(\Delta x^{2r-1}).$$

By Gronwall's inequality, we have (2.25). $\qquad\square$

Remark. In fact, the assumption on the nondegeneracy of K in theorem 2.3 is not necessary. When K is singular, we still have equations corresponding to (2.27) and (2.34) in which first terms on the left sides are vectors with $r \times \text{rank}(\mathsf{K})$ non-zero elements.

Example 2.2. *For the linear wave equation*

$$q_{tt} - q_{xx} = 0, \qquad -1 \leq x < 1, \tag{2.40}$$

we take periodic boundary conditions and initial values taken from the travelling wave solution

$$q(x,t) = e^{\sin(\pi(x-t))}. \tag{2.41}$$

For the nonlinear Sine-Gordon equation

$$q_{tt} - q_{xx} = -\sin q, \qquad 0 \leq x \leq L, \tag{2.42}$$

we use periodic boundary conditions and initial values taken from the travelling wave solution

$$q(x,t) = 2\sin^{-1}(k\,\text{sn}(x - vt)/\sqrt{v^2 - 1}, k^2), \quad L = 4\sqrt{v^2 - 1}K(k^2) \tag{2.43}$$

where K is the complete elliptic integral of the first kind. We have taken parameters $v = 1.5$ and $k = 0.9$. In both cases we use the 4D multi-Hamiltonian formulation [6]

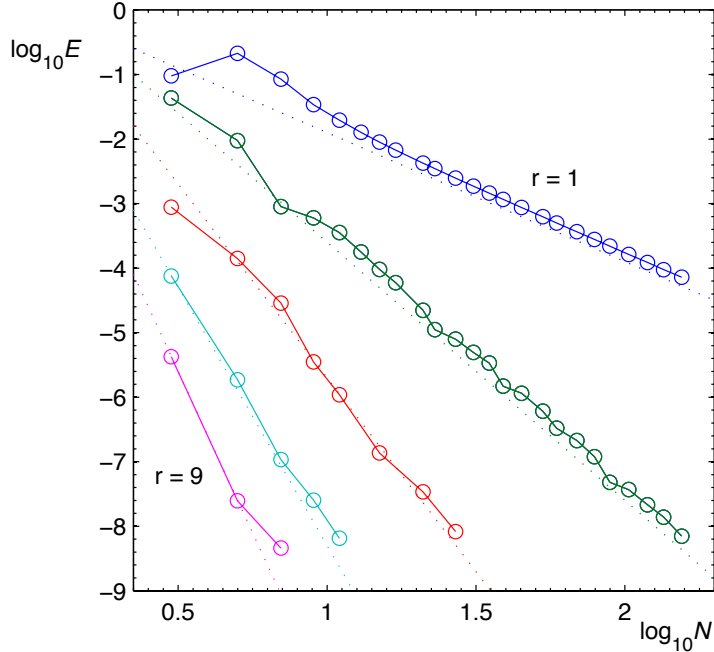$$\mathsf{K}z_t + \mathsf{L}z_x = \nabla S(z), \tag{2.44}$$

Figure 2.5: Global error at $t = 0.1$ of the GLRK spatial discretization with $r = 1, 3, 5, 7$, and 9 stages for the linear wave equation, with periodic boundary conditions and exact solution $q(x, t) = e^{\sin(\pi(x-t))}$, $-1 \leq x < 1$. The number of spatial cells N is chosen to be various odd numbers from 3 to 155. The dotted lines have slopes $r + 1$. The time integration is performed using the implicit mid-point rule with time step 10^{-4}, which ensures that temporal errors and less than spatial errors. The error measure is the weighted 2-norm E defined in (2.25).

with

$$
\mathsf{K} = \begin{bmatrix} 0 & -1 & 0 & 0 \\ 1 & 0 & 0 & 0 \\ 0 & 0 & 0 & 1 \\ 0 & 0 & -1 & 0 \end{bmatrix}, \quad \mathsf{L} = \begin{bmatrix} 0 & 0 & -1 & 0 \\ 0 & 0 & 0 & -1 \\ 1 & 0 & 0 & 0 \\ 0 & 1 & 0 & 0 \end{bmatrix}, \quad \text{and } S(z) = \frac{1}{2}v^2 - \frac{1}{2}w^2 - \cos q
$$

(2.45)

where $z = (q, v, w, \phi)^T$. Initial conditions are given by the exact solution for q, v $(-q_t)$, w $(= q_x)$ evaluated at the stage grid points, and by $\phi = 0$.

In Fig. 2.5 and Fig. 2.6, the r-stage GLRK method is applied to these linear and nonlinear wave equations in space, and the numerical results for the global error are shown for $r = 1, 3, 5, 7$, and 9. The order appears to be $r + 1$ in all cases, which suggests that at least for some initial value problems, the order (r) established in Theorem 2.3 can be exceeded.
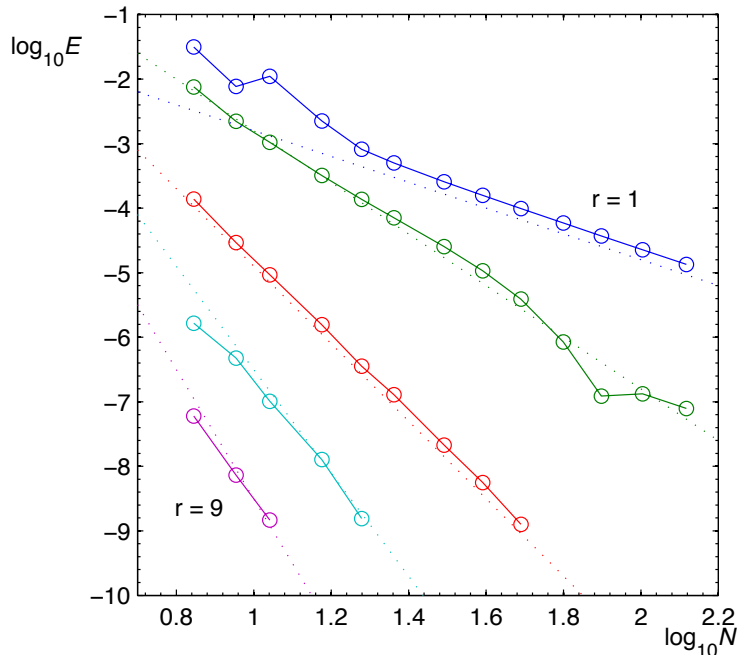
Figure 2.6: Global error at $t = 0.1$ of GLRK spatial discretization with $r = 1, 3, 5, 7$, and 9 stages for the nonlinear Sine-Gordon equation, with periodic boundary conditions and exact solution $q(x,t) = 2\sin^{-1}(k\,\mathrm{sn}(x - vt)/\sqrt{v^2 - 1}, k^2)$, $0 \leq x < L := 4\sqrt{v^2 - 1}K(k^2) \approx 10.2$, $v = 1.5$, $k = 0.9$. The number of spatial cells N is chosen to be various odd numbers from 7 to 131. The dotted lines have slopes $r + 1$. The time integration is performed using the implicit mid-point rule with time step 10^{-4}, which ensures that temporal errors and less than spatial errors. The error measure is the weighted 2-norm E defined in (2.25).

3 Spatial discretization by partitioned Runge–Kutta methods

3.1 Multisymplecticity

Multisymplectic integrators can be obtained using partitioned Runge–Kutta methods [18, 17]. In practice, the choice of partitioning in each dimension depends on the structure of K and L. Conditions ensuring multisymplecticity for 2-part partitioning were obtained in [13]. The following theorem greatly simplifies the result in [13] and extends it to complete N-part partitioning, which includes all other partitionings as special cases. That is, it allows possibly different RK coefficients for each component of the system. The proof uses a technique that is standard in the study of symplectic Runge–Kutta methods and can be found in [16], Theorem 3.2.1.

Theorem 3.1. *The multi-Hamiltonian PDE*

$$\sum_{\alpha=1}^{N} \mathsf{K}^{\alpha} \frac{\partial z}{\partial x_\alpha} = \nabla S(z) \tag{3.1}$$

for $z \colon \mathbb{R}^N \to \mathbb{R}^d$, discretized in each dimension x_α by an r_α-stage fully partitioned Runge–Kutta method, has a discrete multisymplectic conservation law when, for each dimension x_α, the coefficients $(a_{ij}^{(\gamma)}, b_j^{(\gamma)})$ of the PRK method in component $\gamma = 1, \ldots, d$ and dimension x_α satisfy the conditions

$$\begin{aligned} b_j^{(\gamma)} &= b_j, \\ -a_{kj}^{(\gamma)} b_k^{(\beta)} - b_j^{(\gamma)} a_{jk}^{(\beta)} + b_j^{(\gamma)} b_k^{(\beta)} &= 0, \end{aligned} \tag{3.2}$$

for all j, k and for all pairs (β, γ) such that $\mathsf{K}_{\beta\gamma}^{(\alpha)} \neq 0$. The discrete multisymplectic conservation law is then given by

$$\sum_{\alpha=1}^{N} \sum_{\substack{\delta=1 \\ \delta \neq \alpha}}^{N} \sum_{j_\delta=1}^{r_\delta} \prod_{\substack{\epsilon=1 \\ \epsilon \neq \alpha}}^{N} \Delta x_\epsilon b_{j_\delta}^\epsilon \left(\omega_{i_\alpha+1}^{\alpha,j_\delta} - \omega_{i_\alpha}^{\alpha,j_\delta} \right) = 0, \tag{3.3}$$

where $\omega_{i_\alpha}^{\alpha,j_\delta} = \frac{1}{2} \sum_{\beta,\gamma} \mathsf{K}_{\beta\gamma}^\alpha \mathrm{d} Z_{i_\alpha}^{\gamma,j_\delta} \wedge \mathrm{d} Z_{i_\alpha}^{\beta,j_\delta}$ and $b_{j_\delta}^\epsilon$ is the component of coefficient b_{j_δ} in the dimension x_ϵ. This is a natural discretization of the multisymplectic conservation law $\sum_{\alpha=1}^{N} \omega_{,x_\alpha}^\alpha = 0$, $\omega^\alpha = \frac{1}{2} \mathsf{K}^\alpha \mathrm{d} z \wedge \mathrm{d} z$, of the PDE (3.1).

For the PDE (2.1) in one time and one space dimension, by using r-stage PRK in space with weights b_j and s-stage PRK in time with weights B_j, Eq. (3.3) reduces to

$$\Delta x \sum_{j=1}^{r} b_j (\omega_{i,j}^{n+1} - \omega_{i,j}^n) + \Delta t \sum_{n=1}^{s} B_n (\kappa_{i+1}^{n,m} - \kappa_i^{n,m}) = 0$$

which is a numerical quadrature of the integral of $\omega_t + \kappa_x = 0$ over a cell.

3.2 Explicit discretization

The problems of implicit and possibly singular ODEs can be avoided for multi-Hamiltonian PDEs with

$$\mathsf{K} = \begin{bmatrix} & -I_{\frac{1}{2}(d_1+d_2)} & \\ I_{\frac{1}{2}(d_1+d_2)} & & \\ & & O_{d_1} \end{bmatrix}, \quad \mathsf{L} = \begin{bmatrix} & & I_{d_1} \\ & O_{d_2} & \\ -I_{d_1} & & \end{bmatrix}, \tag{3.4}$$

and $S(z) = \frac{1}{2} p^\top \mathsf{A} \mathsf{p} + \mathsf{V}(\mathsf{q}) + \frac{1}{2} \mathsf{v}^\top \mathsf{B} \mathsf{v}$. Here, $d_1 = n - \mathrm{rank}(\mathsf{K})$, $d_2 = n - 2d_1 \leq d_1$, I_d is the $d \times d$ identity matrix, O_d is the $d \times d$ zero matrix, $z = (q, v, p)$, $q, p \in \mathbb{R}^{d_1}$, $v \in \mathbb{R}^{d_2}$,

and A and B are two nonsingular matrices. In Theorem 4.1 of [18], it is shown that a spatial discretization by a PRK method with coefficients satisfying

$$a_{1j} = 0, \ a_{rj} = b_j, \ \hat{a}_{jr} = 0, \ \hat{a}_{j1} = b_1, \quad 1 \leq j \leq r; \tag{3.5}$$

$$\det C \neq 0, \quad C_{i-1,j-1} = \sum_{k,l} a_{ik}(b_l - \delta_{kl})\hat{a}_{lj}, \quad 2 \leq i,j \leq r-1, \tag{3.6}$$

leads to explicit ODEs for the stage variables associated with q [16]. Here the a_{ij}, RK coefficients, are used for the discretization of q_x and the $\hat{a}_{ij}$, RK coefficients, are used for the discretization of p_x; v_x does not appear in the PDE and no approximation of it is needed or used. These PDEs include those such as the nonlinear wave equation and nonlinear Schrödinger equation for which spatial derivatives of order other than 2 can be eliminated.

We concentrate in this paper on the discretization of q_{xx} that results from applying the r-stage Lobatto IIIA–IIIB method. Let E be the $(r-2) \times r$ matrix with nonzero entries

$$E_{k,1} = 1 - c_{k+1}, \quad E_{k,k+1} = -1, \quad E_{k,r} = c_{k+1}$$

for $k = 1, \ldots, r-2$, and let $F_1 = C^{-1}E$. Let $F_2 = (\mathbf{b}^\top - \mathbf{b}^\top \widehat{A})_{2:r-1}$ and $F_3 = (\mathbf{b}^\top \widehat{A})_{2:r-1}$. Then the discretization is given by

$$q_{xx}(x_i + c\Delta x) \approx \frac{1}{(\Delta x)^2} F_1 Q(i), \tag{3.7}$$

$$q_{xx}(x_i) \approx \frac{1}{2b_1(\Delta x)^2} \left(F_2 F_1 Q(i-1) + F_3 F_1 Q(i) + \delta^2 Q_1(i) \right).$$

For the nonlinear wave equation $q_{tt} = q_{xx} - V'(q)$, the semidiscretization leads to the following ODEs

$$\partial_{tt} Q = DQ - V'(Q), \tag{3.8}$$

where D is the difference operator determined by (3.7). When $r = 2$, the spatial discretization (3.7) reduces to central differences. When $r = 3$ we get the explicit system of ODEs

$$\begin{bmatrix} \partial_{tt} Q_1(i) \\ \partial_{tt} Q_2(i) \end{bmatrix} = \frac{1}{(\Delta x)^2} \begin{bmatrix} -1 & 8 & -14 & 8 & -1 \\ 0 & 0 & 4 & -8 & 4 \end{bmatrix} \begin{bmatrix} Q_1(i-1) \\ Q_2(i-1) \\ Q_1(i) \\ Q_2(i) \\ Q_1(i+1) \end{bmatrix} - \begin{bmatrix} V'(Q_1(i)) \\ V'(Q_2(i)) \end{bmatrix}.$$

$$\tag{3.9}$$

When $r = 4$, the corresponding difference stencil approximating ∂_{xx} is

$$\begin{bmatrix} 1 & \frac{1}{2}(25 - 15\sqrt{5}) & \frac{1}{2}(25 + 15\sqrt{5}) & -52 & \frac{1}{2}(25 + 15\sqrt{5}) & \frac{1}{2}(25 - 15\sqrt{5}) & 1 \\ 0 & 0 & 0 & 5 + 3\sqrt{5} & -20 & 10 & 5 - 3\sqrt{5} \\ 0 & 0 & 0 & 5 - 3\sqrt{5} & 10 & -20 & 5 + 3\sqrt{5} \end{bmatrix}.$$

Note that, for any multi-Hamiltonian PDE, either K or L can be put in the form given in (3.4), for this is just the Darboux normal form, so (3.4) amounts to a restriction on just one of K, L. The examples in [16] give an idea of the range of applicability of the method. For equations which are not of the separable form (3.4), such as the Korteweg–de Vries equation, the Lobatto IIIA–IIIB method can still be applied, but it does not lead to explicit ODEs. Instead it gives discretizations like the "narrow box" scheme of [2], which is again implicit, leading to the same drawbacks as the GLRK method.

A treatment of boundary conditions for all multi-Hamiltonian PDEs is difficult because this requires knowing which boundary conditions make the PDE well-posed. However, for equations which can be written in terms of second space derivatives only, boundary conditions appear to be easily handled by the Lobatto IIIA–IIIB method. For Dirichlet boundary conditions the finite difference stencil (3.7) is applied at interior stage points only, giving a closed set of ODEs. For more general (e.g. Robin or outgoing) boundary conditions, the PRK equations in the first cell can be manipulated to yield finite difference approximations for $q_{xx}(x_1)$. For $r = 2$ (central differences) this is standard; for $r = 3$ the approximation is

$$q_{xx}(x_1) \approx -\frac{2}{(\Delta x)^2} \left(7Q_1(1) - 8Q_2(1) + Q_3(1) + 3\Delta x \, q_x(x_1) \right),$$

where $q_x(x_1)$ is determined from the boundary conditions and $Z_1(1)$. (For example, for the wave equation with the outgoing boundary condition $q_t + q_x = 0$ at the left-hand boundary, we set $q_x(x_1) = -q_t(x_1) = -P_1(1)$, where $P_1(1)$ is one of the dependent variables.) In contrast, we have not been able to find a consistent treatment of Dirichlet or Neumann boundary conditions for the Gauss–Legendre Runge–Kutta method that leads to nonsingular implicit ODEs, even for the nonlinear wave equation.

3.3   Dispersion analysis

To analyze the stability of Labotto IIIA–IIIB methods, in [14] we presented two possible model equations, separable and nonseparable; and it is shown there that for multi-Hamiltonian PDEs of the form considered in Section 3, which can be written in terms of second space derivatives only, the separable form determines the stability of spatial semidiscretization. The separable model equation is the harmonic oscillator

$$\begin{bmatrix} q_x \\ p_x \end{bmatrix} = \begin{bmatrix} 0 & k \\ -k & 0 \end{bmatrix} \begin{bmatrix} q \\ p \end{bmatrix}, \tag{3.10}$$

whose exact solution is

$$\begin{bmatrix} q(x) \\ p(x) \end{bmatrix} = \begin{bmatrix} \cos(kx) & \sin(kx) \\ -k\sin(kx) & k\cos(kx) \end{bmatrix} \begin{bmatrix} q_0 \\ p_0 \end{bmatrix}$$

with initial values $q_0 = q(0), p_0 = p(0)$. The solution is the linear combination of two independent solutions, which correspond to the even and odd modes. For (3.10),

21

applying the Lobatto IIIA–IIIB method gives

$$
\begin{bmatrix} q_1 \\ p_1 \end{bmatrix} = M(k\Delta x) \begin{bmatrix} q_0 \\ p_0 \end{bmatrix} = \begin{bmatrix} M_{11} & M_{12} \\ M_{21} & M_{11} \end{bmatrix} \begin{bmatrix} q_0 \\ p_0 \end{bmatrix},
\tag{3.11}
$$

where $M(k\Delta x)$ is the stability matrix with elements M_{ij} the rational functions [14].

Theorem 3.2. *The ODEs determined by applying a PRK method (whose coefficients satisfy (3.5), (3.6)) in space to multi-Hamiltonian PDEs of the form (3.4) (which can be written in terms of second space derivatives), have periodic solutions of the form $Z_j(i) = \exp(\mathrm{i}(\omega t + Ki\Delta x))Y_j$ where*

$$
\frac{1}{2}\mathrm{tr}M(k\Delta x) = \cos(K\Delta x)
\tag{3.12}
$$

and ω and k satisfy (2.16). The method is stable if there are $r-1$ disjoint intervals in $(0,\infty)$ for which $\left|\frac{1}{2}\mathrm{tr}M(k\Delta x)\right| < 1$. Interval endpoints at which $(\mathrm{tr}M(k\Delta x))' \neq 0$ create spurious jumps and critical points in the discrete dispersion relation. The Lobatto IIIA–IIIB pair is stable and all its interval endpoints lead to spurious jumps and critical points.

Proof. See Theorem 4.1 (i) in [14]. □

Thus, for Lobatto IIIA–IIIB, there are no spurious or parasitic waves, but only a *discontinuous portion* of the continuous frequency range is captured. In Fig. 3.1, we show the correspondence between discrete and continuous frequencies established by (3.12) for $r = 2, \ldots, 5$. These also illustrate the discrete dispersion relation obtained when the method is applied to the linear wave equation. Spurious jumps and critical points at $K\Delta x = n\pi$, $n \in \mathbb{Z}$ can be observed. For fixed n they are exponentially small in r as $r \to \infty$ [14], but for $n = \mathcal{O}(r)$ they are significant. The spurious critical point at $K\Delta x = \pi$ which arises when $r = 2$, i.e., for the central difference approximation of z_{xx}, leading for the linear wave equation to wave packets that propagate with speed $\mathcal{O}(\Delta x)$ instead of 1, is known to cause several types of qualitative errors [19]. Internal discontinuities in the dispersion relation have not been studied as far as we know.

For $r=2$, 3, 4, 5, the portion of the continuous frequency range that is captured by the method is that with $k\Delta x$ in the following domains:

- $r = 2$: $(0,2)$;

- $r = 3$: $(0, 2\sqrt{2}) \cup (2\sqrt{3}, 2\sqrt{6})$;

- $r = 4$: $(0, 3.11272) \cup (3.16228, 5.47723) \cup (7.74597, 8.62038)$;

- $r = 5$: $(0, 3.14045) \cup (3.14247, 6.05405) \cup (6.48074, 8.25455) \cup (13.04319, 13.54062)$.

The supremum of these domains determines, for many wave equations, the fastest wave and hence the CFL limit on explicit time-stepping.
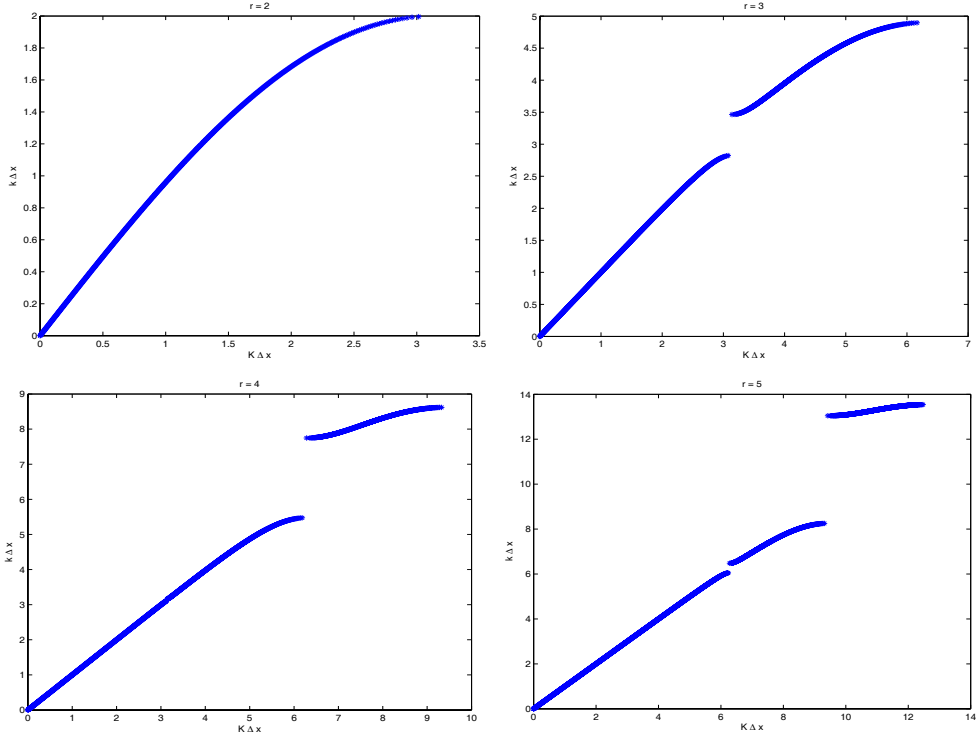
Figure 3.1: Dispersion relations for Lobatto IIIA–IIIB method of $r = 2, 3, 4, 5$ stages. Left top: $r = 2$; Right top: $r = 3$; Left bottom: $r = 4$; Right bottom: $r = 5$.

Our analysis raises the prospect of adding more design criteria to the methods. In addition to multisymplecticity, explicit ODEs, stability, and order, one could add criteria like $\frac{1}{2}\text{tr}M(k^*) = \pm 1$, $\text{tr}M(k^*)' = 0$ (to avoid the discontinuity in the discrete dispersion relation at k^*), or to minimise $\sup\{k^* \colon \frac{1}{2}\text{tr}M(k^*) = \pm 1\}$ (to make the ODEs less stiff and reduce the CFL limit on explicit time-stepping). Note that the Lobatto IIIA–IIIB family was designed for maximum classical order (and hence maximum dispersion order), but this can be sacrificed while preserving the more relevant stage order (see Section 3.4). To demonstrate that this is possible, we construct here one such method that has no jump at $K\Delta x = \pi$, as follows:

- Consider 4-stage PRK methods in which the first member is a collocation method with nodes $(0, c, 1-c, 1)$, and the second method is determined by the symplecticity condition. This ensures a multisymplectic integrator that obeys (3.5), (3.6).

- Calculate $\frac{1}{2}\text{tr}M(k)$ for this class of methods.

- Determine c by solving $\frac{1}{2}\text{tr}M(k^*) = -1$, $\text{tr}M(k^*)' = 0$ for $k^*(\approx \pi)$ and c.

23

This determines $c \approx 0.280123$ as $\frac{1}{2}(1 + d)$ where d is the root (near -0.439753) of

$$39d^{12} - 2298d^{10} + 1209d^8 + 308d^6 - 375d^4 + 102d^2 - 9 = 0.$$

For this method, $\frac{1}{2}\mathrm{tr}M(k)$ has a local minimum of -1 at $k^* \approx 3.14663$, so there is no jump in the discrete dispersion relation at $K\Delta x = \pi$. This method only has dispersion order 2. This can be increased by adding more stages. With $r = 5$, nodes $(0, c, \frac{1}{2}, 1-c, 1)$, there is a method with $c \approx 0.174245$ which has of dispersion order 4 and no jump in the discrete dispersion relation at $K\Delta x = \pi$.

We turn now to determining the discrete modes or eigenfunctions. These now have two components, Q_j and P_j, each with an odd and an even mode which are determined by solving

$$\begin{bmatrix} I_r & -kA \\ k\widehat{A} & I_r \end{bmatrix} \begin{bmatrix} Q \\ P \end{bmatrix} = \begin{bmatrix} \mathbf{1}_r q_0 \\ \mathbf{1}_r p_0 \end{bmatrix} \tag{3.13}$$

with initial values (p_0, q_0), where $\widehat{A}$ and A are the matrices corresponding to the Lobatto IIIA–IIIB pair. It follows by eliminating P from (3.13) that

$$Q = (I_r + k^2 \Delta x^2 A\widehat{A})^{-1}(k\Delta x A \mathbf{1}_r p_0 + \mathbf{1}_r q_0). \tag{3.14}$$

We use a basis $(p_0, q_0) = (0, 1)$ and $(p_0, q_0) = (1, \sin(K\Delta x)/k\Delta x)$ for the two independent computational modes. When $r = 2$, the even mode is $Q = (1, \cos(K\Delta x))^\top$ and the odd mode is $Q = (0, \sin(K\Delta x))^\top$ which coincide with the corresponding continuous modes. With $r = 3$ the even mode approximating for small $K\Delta x$ the continuous mode $q_j = \cos(Kc_j\Delta x)$, is

$$Q = \begin{bmatrix} 1 \\ \dfrac{2(12 - k^2\Delta x^2)}{24 + k^2\Delta x^2} \\ \cos(K\Delta x) \end{bmatrix}; \tag{3.15}$$

The odd mode approximating the continuous mode $q_j = \sin(Kc_j\Delta x)$, is

$$Q = \begin{bmatrix} 0 \\ -\dfrac{4\sin(K\Delta x)}{k^2\Delta x^2 - 8} \\ \sin(K\Delta x) \end{bmatrix}. \tag{3.16}$$

We show the even and odd modes for $r = 3, 4, 5$ in Figs. 3.2–3.4. As with the results for GLRK (Figs. 2.3, 2.4), it appears that the first half of the frequency spectrum is converging as $r \to \infty$. The discrete modes do not uniformly approximate the continuous modes as $K\Delta x \to n\pi$, $n \in \mathbb{Z}$; we do not know if this has implications for the numerical performance of these methods.
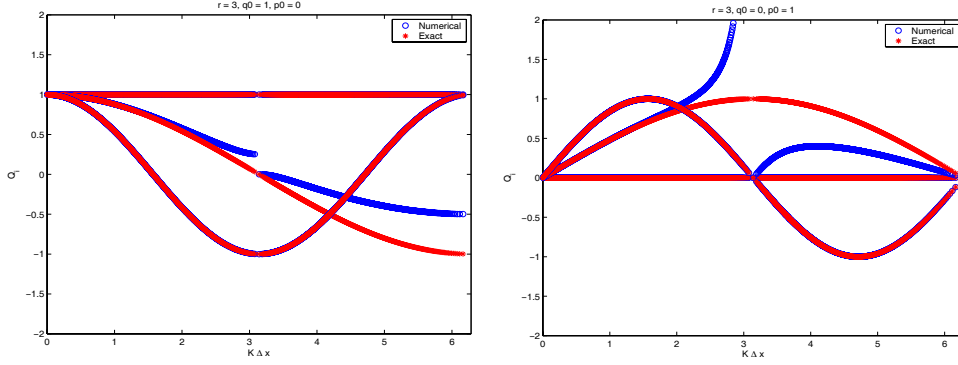
Figure 3.2: Numerical modes $\{Q_i\}_{i=1}^3$ with respect to $K\Delta x$ for 3-stage Lobatto IIIA-IIIB pair. Left: Even mode corresponding to $(p_0, q_0) = (0, 1)$; Right: Odd mode corresponding to $(p_0, q_0) = (1, \sin(K\Delta x)/k\Delta x)$. The $*$ lines denote the exact modes.
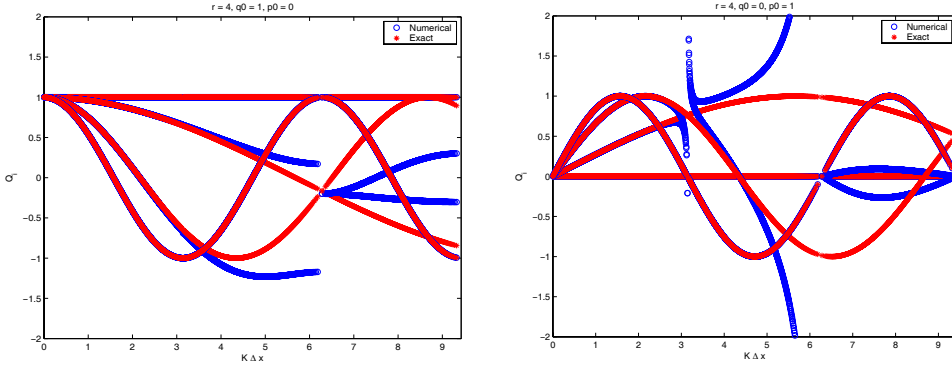

Figure 3.3: Numerical modes $\{Q_i\}_{i=1}^4$ with respect to $K\Delta x$ for 4-stage Lobatto IIIA-IIIB pair. Left: Even mode corresponding to $(p_0, q_0) = (0, 1)$; Right: Odd mode corresponding to $(p_0, q_0) = (1, \sin(K\Delta x)/k\Delta x)$. The $*$ lines denote the exact modes.

3.4 Global error

The dispersion order of r-stage Lobatto IIIA–IIIB method is the same as its classical order, namely $2r - 2$, which is shown in the following proposition.

Proposition 3.1. *When $k\Delta x$ is sufficiently small, the error in the numerical dispersion is*

$$K\Delta x - k\Delta x = \frac{1}{2r - 2}e_{r-1}(k\Delta x)^{2r-2} + \mathcal{O}((k\Delta x)^{2r}), \qquad (3.17)$$

where $e_r := \frac{r!^2}{(2r)!(2r+1)!}$.

Proof. The error estimate (3.17) can be obtained from Proposition 8.1 in [14]; it is also shown in [1]. $\qquad\square$
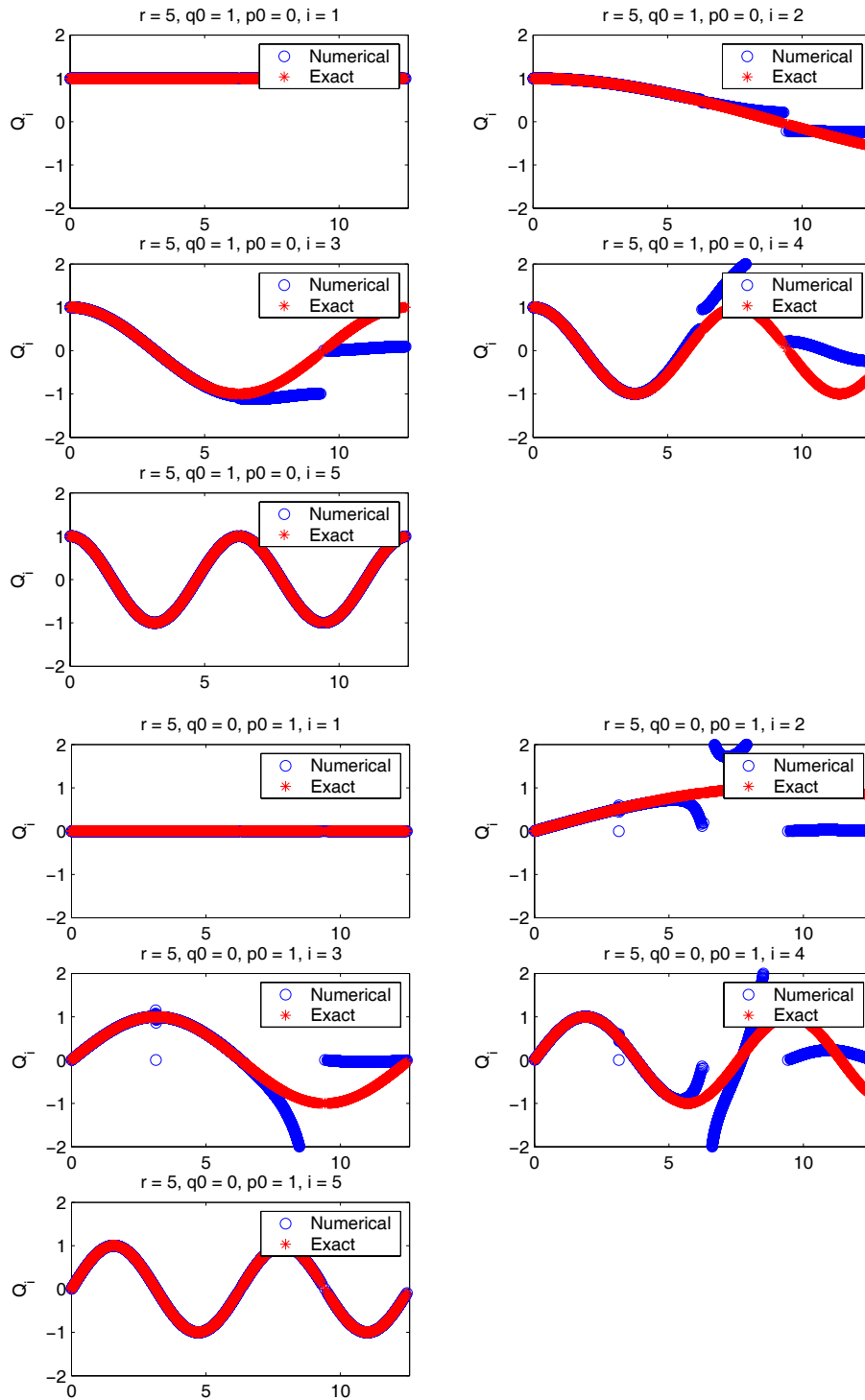
Figure 3.4: Numerical modes $\{Q_i\}_{i=1}^5$ with respect to $K\Delta x$ for 5-stage Lobatto IIIA-IIIB pair. Top: Even modes; Bottom: Odd modes. The $*$ lines denote the exact modes.
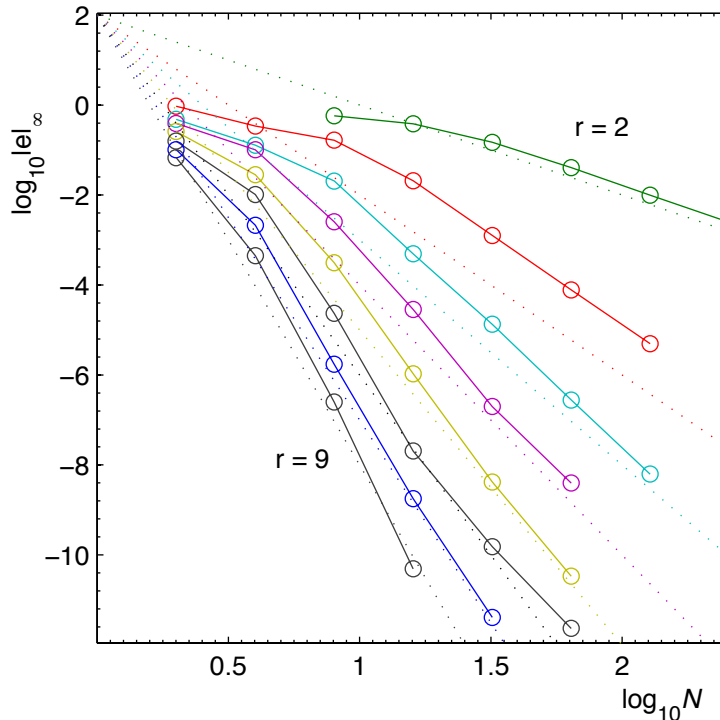
Figure 3.5: Global error at $t = 0.1$ of Lobatto IIIA–IIIB spatial discretization for the linear wave equation $q_{tt} = q_{xx}$, $0 \leq x < 2\pi$, with periodic boundary conditions. The exact solution is $q(x, t) = \exp(5(\sin(x + t) - 1))$, and $N = 2, 4, 8, 16, \ldots, 256$ is the number of spatial cells. The dotted lines have slopes given by the observed order of the global error, namely 2 for $r = 2$ and $r + 1$ for $r \geq 3$. The time integration is performed using a Krylov method for the matrix exponential and is exact up to roundoff. The error measured is the maximum absolute error in q over all stage variables $Q_j(i)$.

However, the order of the local truncation error is lower than the dispersion order when $r > 2$. Here, we define the 'local truncation error' in terms of a mapping from smooth functions to grid functions; the simplest such mapping, namely evaluation at the collocation points, is used in the following result.

Proposition 3.2. *With $Z_j(i) = z(x_i + c_j \Delta x)$, the local truncation error of the Lobatto IIIA–IIIB discretization of z_{xx} is*

$$
\begin{aligned}
&\mathcal{O}\left((\Delta x)^2\right), && r = 2, \\
&\mathcal{O}\left((\Delta x)^{r-1}\right), && 3 \leq r \leq 10.
\end{aligned}
\tag{3.18}
$$

Proof. Taylor series applied to the finite difference stencils given in Eq. (3.7) allow the local truncation error to be calculated for any value of r; we have carried this out for $2 \leq r \leq 10$, with the given result. □
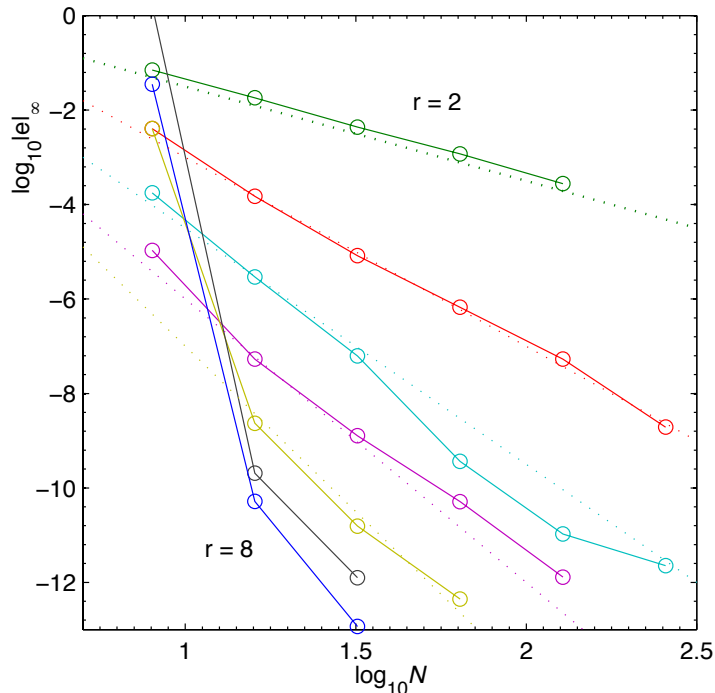
27

Figure 3.6: Global error at $t = 1$ of Lobatto IIIA–IIIB spatial discretization of the sine–Gordon equation $q_{tt} = q_{xx} - \sin q$, $0 \leq x < L$, with periodic boundary conditions, for the exact solution $q(x, t) = \pi - 2\phi((x - vt)/(k\sqrt{1 - v^2}), k^2)$, $L = 2k\sqrt{1 - v^2}K(k^2)$; ϕ is the Jacobi amplitude function, K is the complete elliptic integral of the first kind, $v = 0.5$, and $k = 0.99$. There are $N = 4, 8, 16, \ldots, 256$ spatial cells. Time integration is done using a 4th order symplectic splitting method, with time step small enough that the global error is dominated by the spatial error. The dotted lines have slopes given by the observed order of the global error, namely 2 for $r = 2$ and $r + 1$ for $r \geq 3$. The error measured is the maximum absolute error in q over all stage variables $Q_j(i)$.

Numerical simulations of the linear and nonlinear wave equations with periodic boundary conditions are shown in Fig. 3.5 and Fig. 3.6. The observed global error is

$$\begin{aligned} \mathcal{O}\left((\Delta x)^2\right), & \quad r = 2. \\ \mathcal{O}\left((\Delta x)^{r+1}\right), & \quad 3 \leq r \leq 8. \end{aligned} \tag{3.19}$$

which is of *higher* order than the local truncation error!

We do not have an explanation for this phenomenon. However, for linear equations there is a mapping of continuous to grid functions (derived from the discrete eigenfunctions) that makes the local truncation error equal to the dispersion order. This is not expected to be possible for nonlinear equations, but it suggests the following.

Proposition 3.3. *With smooth functions $z(x)$ mapped to grid functions by $Z_j(i) = $*

$(1+a_j(\Delta x)^4\partial_x^4)z(x_i+c_j\Delta x)$, $a_1 = 0$, and $a_2 = \frac{1}{384}$, *the principal local truncation error of z_{xx} at $x_i+c_j\Delta x$ by the 3-stage Lobatto IIIA–IIIB discretization is $\hat{a}_j(\Delta x)^4\partial_x^6 z(x_i+c_j\Delta x)$ with $\hat{a}_1 = \frac{1}{360}$ and $\hat{a}_2 = \frac{1}{5760}$, that is, it is a 4th order finite difference to z_{xx}.*

With smooth functions $z(x)$ mapped to grid functions by $Z_j(i) = (1+a_j(\Delta x)^5\partial_x^5)z(x_i+ c_j\Delta x)$ with $a_1 = a_4 = 0$, $a_2 = -a_3 = -1/(9000\sqrt{5})$, the principal local truncation error of z_{xx} by the 4-stage Lobatto IIIA–IIIB discretization is $\hat{a}_j(\Delta x)^5\partial_x^7 z(x_i + c_j\Delta x)$ with $\hat{a}_1 = \hat{a}_4 = 0$, $\hat{a}_2 = -\hat{a}_3 = -\frac{1}{302400}$, that is, it is a 5th order finite difference.

Proof. The proof is by Taylor series expansions. At $j = 1$,

$$\frac{1}{(\Delta x)^2}\left(-14Z_1(i) + 8(Z_2(i) + Z_2(i-1)) - (Z_1(i+1) + Z_1(i-1))\right)$$
$$= \left(\partial_x^2 - \tfrac{1}{24}(\Delta x)^2(1 + 384a_1 - 384a_2)\partial_x^4 + (\Delta x)^4(\tfrac{-7}{2800} - a_1 + 2a_2)\partial_x^6\right)z(x_i),$$

$$\frac{1}{(\Delta x)^2}\left(4Z_1(i) - 8Z_2(i) + 4Z_1(i+1)\right)$$
$$= \left(\partial_x^2 + (\Delta x)^2(\tfrac{1}{48} + 8a_1 - 8a_2)\partial_x^4 + (\Delta x)^4(\tfrac{1}{5760} + a_1)\partial_x^6\right)z(x_i + \tfrac{1}{2}\Delta x).$$

Setting the coefficients of $(\Delta x)^4$ equal to zero determines the values of a_1 and a_2 given in the proposition. The calculation is similar for $r = 4$. $\qquad\square$

Therefore, under this mapping of smooth functions to grid functions, the global error is necessarily of order $r + 1$ for $r = 3, 4$. We expect that a similar modification of the initial conditions leads to a local truncation error and global error of order $r + 1$ for all $r \geq 3$.

The unexpected numerical observation is that even *without* this modification of the grid functions, the observed global order is still $r + 1$ and not $r - 1$. In some way the Z_js adjust themselves during the time evolution so as to reduce the global error. The modified and unmodified methods are shown in Figure 3.7; the modified method is smoother in time and has slightly smaller global error in this example.

The order of the global error we have observed here is, for $r > 2$, one higher than that claimed in [7], Table 11.3, for the same method with unmodified initial conditions applied to the homogeneous linear wave equation.

Note that there are only $r - 1$ dependent variables per cell, so this observed order is 2 higher than that established in Theorem 2.3 for GLRK for the same number of degrees of freedom. This may be the most accurate possible class of finite difference methods for this class of equations.

4   Conclusion

The families of methods considered here have outstanding numerical properties in terms of order, preservation of the dispersion relation, lack of parasitic waves, and multisymplecticity which can be expected to lead to good long-time behaviour and good preservation of qualitative solution properties. It is striking and unfortunate that the method
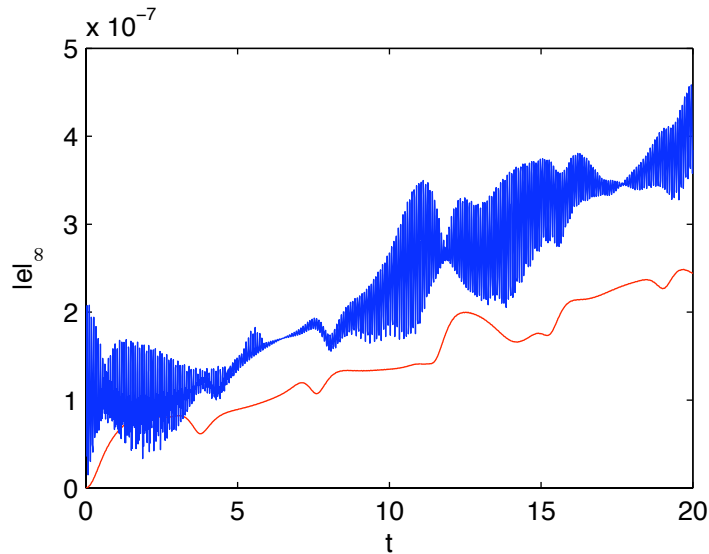
Figure 3.7: Global error as a function of time for the sine–Gordon problem shown in Figure 3.6 with initial conditions $Z_j(x_i) = (1+a_j\Delta x)^4\partial_x^4)z(x_i+c_j\Delta x)$. Red line: modified initial conditions $a_1 = 0$, $a_2 = \frac{1}{384}$, known to be 4th order. Blue line: unmodified initial conditions $a_1 = a_2 = 0$, observed to be 4th order. Here there are $N = 100$ spatial cells, the time step is 0.01, and the time integrator is a 4th order symplectic splitting method.

which might be expected to be best overall, namely Gauss–Legendre Runge–Kutta, and which is the most-used example of a multisymplectic integrator in the literature, has a number of glaring weaknesses: it leads to (at best) implicit ODEs; these can be singular; and no general treatment of boundary conditions is known. If the latter two issues can be overcome, then dealing with the implicit ODEs is not an insuperable obstacle.

In contrast, the Lobatto IIIA–IIIB method has a number of additional definite advantages: it can lead to explicit ODEs, allowing explicit multisymplectic time-integration; and it has the apparently best possible order behaviour. An apparent drawback, that the dispersion relation can have spurious jumps and critical points, is of uncertain practical impact: this should be investigated further. Other open problems for this method include analysis of the discrete eigenfunctions for $r \to \infty$, determining if the observed order of the global error is the actual order, and if so, understanding the mechanism by which this is achieved.

References

[1] M. AINSWORTH AND H. A. WAJID, *Dispersive and dissipative behavior of the spectral element method*, SIAM J. Numer. Anal., 47 (2009), pp. 3910–3937.

[2] U. M. ASCHER, *Numerical methods for evolutionary differential equations*, vol. 5

of Computational Science & Engineering, Society for Industrial and Applied Mathematics (SIAM), Philadelphia, PA, 2008.

[3] U. M. ASCHER AND R. I. McLACHLAN, *Multisymplectic box schemes and the Korteweg–de Vries equation*, Applied Numerical Mathematics, 48 (2004), pp. 255–269.

[4] ——, *On symplectic and multisymplectic schemes for the KdV equation*, Journal of Scientific Computing, 25 (2005), pp. 83–104.

[5] T. J. BRIDGES AND S. REICH, *Multi-symplectic integrators: numerical schemes for Hamiltonian PDEs that conserve symplecticity*, Phys. Lett. A, 284 (2001), pp. 184–193.

[6] ——, *Numerical methods for Hamiltonian PDEs*, J. Phys. A, 39 (2006), pp. 5287–5320.

[7] G. C. COHEN, *Higher-order numerical methods for transient wave equations*, Scientific Computation, Springer-Verlag, Berlin, 2002. With a foreword by R. Glowinski.

[8] J. FRANK, B. E. MOORE, AND S. REICH, *Linear PDEs and numerical methods that preserve a multisymplectic conservation law*, SIAM J. Sci. Comput., 28 (2006), pp. 260–277 (electronic).

[9] J. FRANK AND S. REICH, *On spurious reflections, nonuniform grids and finite difference discretizations of wave equations.* CWI Report MAS-E0406, Center for Mathematics and Computer Science, 2004.

[10] N. GUGLIELMI AND E. HAIRER, *Order stars and stability for delay differential equations*, Numer. Math., 83 (1999), pp. 371–383.

[11] E. HAIRER, S. P. NØRSETT, AND G. WANNER, *Solving Ordinary Differential Equations. I*, vol. 8 of Springer Series in Computational Mathematics, Springer-Verlag, Berlin, second ed., 1993. Nonstiff problems.

[12] E. HAIRER AND G. WANNER, *Solving Ordinary Differential Equations. II*, vol. 14 of Springer Series in Computational Mathematics, Springer-Verlag, Berlin, second ed., 1996. Stiff and differential-algebraic problems.

[13] J. HONG, H. LIU, AND G. SUN, *The multi-symplecticity of partitioned Runge-Kutta methods for Hamiltonian PDEs*, Math. Comp., 75 (2006), pp. 167–181 (electronic).

[14] R. I. McLACHLAN, Y. SUN, AND P. S. P. TSE, *Linear stability of partitioned Runge-Kutta methods*, SIAM J. Numer. Math., 49 (2011), pp. 232–263.

[15] S. REICH, *Multi-symplectic Runge-Kutta collocation methods for Hamiltonian wave equations*, J. Comput. Phys., 157 (2000), pp. 473–499.

[16] B. N. Ryland, *Multisymplectic Integration*, PhD thesis, Massy University, New Zealand, 2007.

[17] B. N. Ryland and R. I. McLachlan, *On multisymplecticity of partitioned Runge-Kutta methods*, SIAM J. Sci. Comput., 30 (2008), pp. 1318–1340.

[18] B. N. Ryland, R. I. McLachlan, and J. Frank, *On the multisymplecticity of partitioned Runge–Kutta and splitting methods*, Int. J. Comput. Math., 84 (2007), pp. 847–869.

[19] E. Zuazua, *Propagation, observation, control and numerical approximations of waves*, SIAM Review, 47 (2005), pp. 197–243.